Heat transfer through a water spray curtain under the effect of a strong radiative source

P. Boulet, Anthony Collin, Gilles Parent

Heat transfer through a water spray curtain under the effect of a strong radiative source

P. Boulet*, A. Collin & G. Parent

Laboratoire d'Energétique et de Mécanique Théorique & Appliquée (LEMTA), CNRS UMR 7563

Faculté des Sciences et Techniques BP 239 - 54506 VANDOEUVRE Cedex

Tel & Fax (33) 383 684 686 - mail Pascal.Boulet@lemta.uhp-nancy.fr

Keywords : *heat transfer, radiative transfer, vaporization, convection, water spray*

Abstract

Heat transfer inside a participating medium, made of droplets flowing in gas, receiving a strong irradiation on one side has been studied. Conditions investigated are similar to applications of water spray curtains as fire protection systems. The radiative part has been treated using a Discrete Ordinates Method combined with a c-K model in order to accurately deal with the problem of acute anisotropic scattering and strong wavelength dependence of absorption in gas. Coupling with the energy balance has been introduced using an iterative numerical solution. Various and combined effects due to radiative transfer, conduction, convection, turbulent diffusion and vaporization have been taken into account. This has been achieved introducing realistic dynamic data available in the literature and simultaneously solving a supplementary balance for the moisture inside the spray. Both diffuse and collimated irradiation have been considered. Various configurations have been studied from single sprays to multiple nozzle devices. The temperature level has been found to remain close to the one of the surrounding medium despite the large radiation absorption, as a consequence of competing effects between vaporization, convection and radiative transfer. The role of each term in the balance has been investigated indicating the need for further developments aimed at the accurate simulation of combined mass, momentum and heat transfer in the spray.

*corresponding author

Nomenclature

- B_m, mass Spalding number
- C_p, heat capacity ($J.kg^{-1}.K^{-1}$)
- d, droplet diameter (m)
- $\mathcal{D}$, diffusion coefficient of water vapor in air ($m^2.s^{-1}$)
- f_v, droplet volume fraction (m^3 of water/m^3 of air)
- f_{H_2O}, water vapor volume fraction (m^3 of gas/m^3 of air)
- f_{CO_2}, carbon dioxide volume fraction (m^3 of gas/m^3 of air)
- H, height of the medium (m)
- k_c, thermal conductivity ($W.m^{-1}.K^{-1}$)
- $I^0_\lambda(T)$, blackbody spectral intensity at temperature T ($W.m^{-3}.sr^{-1}$)
- I_λ, spectral intensity ($W.m^{-3}.sr^{-1}$)
- L, width of the medium (m)
- L_v, latent heat of vaporization ($J.kg^{-1}$)
- m_{ev}, vaporization mass flow rate for a single droplet ($kg.s^{-1}$)
- n_λ, spectral refractive index
- N_d, droplet density number (m^{-3})
- P_λ, scattering phase function
- $\vec{q_k}$, conductive flux ($W.m^{-2}$)
- $\vec{q_r}$, radiative flux ($W.m^{-2}$)
- $\vec{q_t}$, turbulent heat flux ($W.m^{-2}$)
- $\dot{Q}$, heat source or loss ($W.m^{-3}$)

- r, droplet radius (m)
- s, position in the medium (m)
- T, temperature (K)
- T', fluctuating temperature (K)
- $\vec{V}$, fluid velocity $(m.s^{-1})$
- v', fluctuating velocity $(m.s^{-1})$
- x, y, z, space co-ordinates (m)
- $Y(z)$, moisture (kg of water/kg of dry air)

Greek symbols

- κ, absorption coefficient (m^{-1})
- ρ, density $(kg.m^{-3})$
- σ, scattering coefficient (m^{-1})
- θ, scattering angle (rad)
- Ω, solid angle (sr)
- $\vec{\Omega}$, propagation direction

Subscripts

- c, continuous phase property
- d, droplet property
- λ, spectral property

1 Introduction

Water sprays are used as protection devices against fire, in various configurations. What we are dealing with in the present study is a water curtain used as a thermal shield (see Figure 1). The spray will be located in

front of a target to be protected, but assumed to be sufficiently far from the fire area to avoid any interaction with flames, except with the strong energy they are radiating. Expected attenuation of this heat flux will be due to the spray ability to weaken a strong irradiation as a consequence of scattering and absorption induced phenomena.

Radiation emitted by the flame will indeed interact with the medium made of a suspension of fine droplets injected in wet air, both phases exchanging in a complex manner, mass, momentum and heat. Therein, water droplets, with size ranging from few tens to few hundreds micrometers, exhibit strong absorbing and anisotropic scattering abilities, whereas water vapor and carbon dioxide only absorb radiation with sharp wavelength-dependent variations. This complex radiative behavior has received much attention, the problem being addressed with various complexity levels. Among the relatively recent studies available in the literature, one may cite the pioneering work by Ravigurajan and Beltran [1], who simulated the temperature increase of a plate exposed to a strong radiative source but protected using a sprinkler-induced spray. If coupling with energy balance for the target was addressed, radiative transfer was solely described on the basis of Beer's law. Results especially allowed a first sensitivity analysis of the droplet size influence. Using an improved radiative model, Coppalle *et al.* [2], Pretrel [3] and Dembélé *et al.* [4] - [5] addressed the problem of thermal shield, the first two references introducing two-flux models and the two others a more accurate Discrete Ordinates Method. In Dembélé *et al.* [6] comparisons were also carried out on the limitations due to simplified formulations of the radiative transfer problem. Only few results are given on combined heat transfer in the spray, however. Even if the studies by Pretrel and Dembélé have been presented as potentially combined to lead to a complete one-dimensional spray description, very few results have been given in such a complex configuration. Moreover a multi-dimensional simulation tool should be developed in order to address the particular difficulty of lateral wind effects.

In a more general frame, recent reviews by Grant *et al.* [7] and by Sacadura [8] deal with the topic of water spray used as protection tools. Reference [7] particularly provides information on spray characteristics and reference [8] presents the state of the art in the field of fire safety science. In addition, complementary information may be also obtained in Grosshandler et al. [9] on water spray characteristics (protection ability being here associated to fire extinction, which shifts the problem from our present focus, where as above mentioned the spray does not interact with flames directly).

The present study is a second step in a work dedicated to detailed modeling of the whole problem. Berour *et al.* [10] recently conducted a study of combined radiative and conductive transfer inside a spray, coupling a

two-dimensional Discrete Ordinates Method (DOM) with a simple energy balance. The predicted temperature levels in the spray were found to be strongly overestimated due to the absence of heat losses like the vaporization phenomena and the convection inside the spray. However, the suitability of an iterative scheme associating a fine solution for the Radiative Transfer Equation (RTE) and the energy balance in a multi-dimensional study was investigated. In the present work, the radiative problem solution has been further improved (including a sharper spectral treatment of gas absorption and a phase function renormalization) and the energy balance has been rewritten featuring complementary transfer phenomena. In particular, based on a review of available experimental results (see Pretrel [3] and Zimmer [11]) the following transfer phenomena are taken into account in our energy balance: radiation, conduction, vaporization of droplets, convection due to droplet injection and consequently driven air flow and turbulent diffusion. The complete heat transfer problem is still addressed uncoupled from the dynamics of the spray. All needed dynamic characteristics may be taken from experimental data available in the literature, except for the mass balance for the liquid phase which could be more relevant if computed with a complementary equation, instead of being simply evaluated as an arbitrary value. Actually, the energy balance is expected to be strongly affected by droplet vaporization, considering the large value of the latent heat. Care is therefore required. Since the temperature and the moisture inside the spray are computed, their inhomogeneous distributions are taken into account in the RTE solution.

The next step will be the simulation of the whole problem of combined mass, momentum and energy balance, which in the frame of two-phase flow will be a hard task however.

In the next paragraph the formulation will be presented, especially detailing the way in which convection, vaporization and turbulence terms are treated. Solving the RTE will be also discussed. Then, the numerical handling based on an iterative process will be presented. Results will be expressed in terms of transmissivity and temperature distributions. Particular attention will be focused on the relative influence of all terms involved in the energy balance, in order to observe the most prominent phenomena. Some information will also be given on the way multiple nozzle solutions may improve the suitability of water spray curtains to behave as fire protection devices.

[Figure 1 about here.]

2 Formulation

2.1 Test case description and assumption discussion

Let us consider a target receiving a radiative flux from a fire area, simulated as a high temperature blackbody source. The water curtain will be supposed to behave as a thermal shield in order to attenuate the radiation received on one side. The spray is assumed to be relatively far from the fire, so that a mixing of droplets in wet air injected in steady air would be a realistic description of the actual spray, a conic shape being assumed. As mentioned in the introduction, our focus here is a study of the radiative transfer coupled with the energy balance. Some shortcuts are used for the dynamics at this stage, but the results obtained will be analysed for the actual roles of the competing effects involved, so that the code will be ready to use more accurate data on the spray flow in a second step. Since it is considered as a strong drawback of the present study, all introduced variables for the flow description will be carefully chosen on the basis of available experimental values. Present numerical results are consequently protected from inaccuracies which come from a strong misinterpretation of the input dynamic data. However, this will lead to some assumptions that we will discuss before describing the corresponding submodels introduced in our simulation.

- The problem will be treated in the yz plane (see Figure 1), assuming that transfer in the x direction can be omitted. The flow is directed downwards in the z direction, whereas the radiative transfer is mainly directed in the y direction. Of course, strong coupled phenomena will occur and will be investigated using our 2D description.

- Dynamic characteristics, namely mean and fluctuating velocities, will be supposed to be constant in the whole curtain. Actual spatial variation of droplet concentration and velocities are not available, but we will assume at least an average behavior of the spray.

- The real conic shape of the spray will not be addressed, since constant velocity assumption will infer a constant falling section for the spray, as if it was of rectangular shape. This is not a realistic geometrical description below the injection point, but it is a reasonable assumption far from the nozzle according to some spray descriptions (e.g. in [3]). Actually, this is required by the conservation of the water flow rate that would hold if vaporization process was not taken into account. Consequently, local droplet concentrations are not exact, but the average droplet volume fraction as a function of the vertical position is correct. This is essential since it is a key characteristic governing the optical depth of the curtain.

- The spray is considered as a two-phase flow of wet air with droplets uniformly distributed, taking into account a realistic size distribution, but considering that the particle diameters are not altered by any process (collision or vaporization for example). Actually, vaporization will be only considered since it induces a heat loss in the medium and a modification of the water vapor concentration. Consequently, radiative properties will be updated during the calculations, but only varying due to the inhomogeneous gas concentrations. Actually it is not yet possible to deal with an heterogeneous droplet concentration without simulating the actual dynamics of the spray, but average volume fraction will be satisfied at each vertical position.

As detailed in the following sections the simulation of the problem will finally involve a simultaneous solution for the energy balance, the moisture balance and the Radiative Transfer Equation.

2.2 Energy balance

Evaluating the different contributions to the heat transfer in the spray considered as a whole, the energy balance may be written as follows:

$$\rho_d.C_{pd}\left(\vec{V_d}.\vec{\nabla}T_d\right) + \rho_c.C_{pc}\left(\vec{V_c}.\vec{\nabla}T_c\right) = -\vec{\nabla}.\vec{q_r} - \vec{\nabla}.\vec{q_k} - \vec{\nabla}.\vec{q_t} + \dot{Q} \tag{1}$$

$\vec{V}$ and T stand for the velocity field and the temperature of a given phase (d and c referring to droplet and continuous phase properties respectively), ρ and C_p correspond to the density and the heat capacity. $\vec{q_r}$, $\vec{q_k}$ and $\vec{q_t}$ designate the radiative, conductive and turbulent heat fluxes. Finally $\dot{Q}$ is a heat source or loss term. The left hand side of the equation corresponds to the convection terms for the droplets and the continuous phase respectively. At this stage, temperature and velocity for both phases are still discriminated, but as commonly assumed in uncoupled heat transfer studies, we will suppose that the distributions for all phases are identical. That means: $T_d = T_c = T$ and $V_d = V_c = V$. This is probably not exact in the area very close to the injection point. However, Pretrel [3] has demonstrated that both phases are very quickly in equilibrium due to momentum and heat exchanges. This makes the previous assumption not far from being realistic. The first term on the right hand side corresponds to the divergence of the radiative flux, that will require the solution of the RTE to be computed. The second term is the common conduction contribution, which will be evaluated, using Fourier's law, featuring a heat conductivity which is the one for wet air (considering that the dispersed phase yields no contribution to heat conduction, collisions between droplets being to scarce and ineffective in what concerns

the heat transfer). The third term is for the turbulent heat flux, which may affect the heat transfer owing to possibly strong induced continuous phase turbulence. Finally, the last term on the right hand side features all remaining possible heat sources or losses. This corresponds here to the latent heat of vaporization.

Let us now detail the way in which each term is handled:

- The convection term is finally written in a straightforward way, since the velocity is supposed to be unidirectional in the z direction and both phases have equal temperatures and velocities:

$$\rho_d.C_{pd}\left(\vec{V_d}.\vec{\nabla}T_d\right) + \rho_c.C_{pc}\left(\vec{V_c}.\vec{\nabla}T_c\right) \approx \rho.C_p.V\frac{\partial T}{\partial z}; \tag{2}$$

  The properties of the equivalent medium under consideration are computed as classical bulk properties:

$$\rho = f_v.\rho_d + (1 - f_v).\rho_c \tag{3}$$

$$C_p = \frac{f_v.\rho_d.C_{pd} + (1 - f_v).\rho_c.C_{pc}}{f_v.\rho_d + (1 - f_v).\rho_c} \tag{4}$$

  where f_v is the volume fraction of droplets in the spray.

  Note that in our test cases, the actual properties of the mixture are mainly governed by air, since a rough value for the droplet volume fraction is 10^{-5} or 10^{-6} m^3 of water $/m^3$ of air .

- The radiative flux divergence is computed as the balance between emitted and absorbed radiation in the following form:

$$\vec{\nabla}.\vec{q_r} = \int_{\lambda=0}^{\infty} \kappa_\lambda \left[4\pi.n_\lambda^2.I_\lambda^0(T(s)) - \int_{\Omega=4\pi} I_\lambda(s,\vec{\Omega}).d\Omega\right].d\lambda \tag{5}$$

  κ_λ is the spray equivalent absorption coefficient, $I_\lambda(s,\vec{\Omega})$ is the spectral intensity at a given position s and $I_\lambda^0(T(s))$ is the blackbody intensity at temperature T. Owing to possible instabilities which may arise when computing source terms in a finite volume scheme, this term will be linearized as explained later in the paragraph devoted to the numerical handling.

- The conductive flux is

$$\vec{q_k} = -k_c.\vec{\nabla}T \tag{6}$$

  where a linear law as a function of temperature has been introduced for the gas conductivity k, in order to approximately fit experimental data reported in [12]. The following correlation has been used:

$$k_c = 6.10^{-5}.T + 8.9 \times 10^{-3} \tag{7}$$

(the temperature being introduced in Kelvin).

This formulation does not require any specific sensitivity study, since laminar diffusion will be overwhelmed by turbulent diffusion in the coming test cases.

- The turbulent flux would require a closure scheme aimed at the simulation of turbulence, which would strongly increase the complexity of the present simulation focused on heat transfer. A zero-equation closure model has therefore been applied, using the so-called Generalized Gradient Diffusion Hypothesis as presented by Rokni and Sunden [13]. As convection is assumed to be largely predominant in the z direction, turbulent diffusion is only addressed in the transverse direction (y). That leads to the following formulation:

$$q_t = \overline{v'.T'} = -C_t.\overline{v'^2}.\frac{k}{\epsilon}.\frac{\partial T}{\partial y} \tag{8}$$

  As can be seen the variance of the fluctuating velocity ($\overline{v'^2}$) has to be introduced, C_t is a modeling constant (for which a value of 0.3 has been suggested by Rokni and Sunden) and k/ϵ features a characteristic time for the turbulence, which is finally computed as the ratio of a characteristic length for the largest turbulent structure l and the fluctuating velocity v'. For l we have used the width of the curtain (L) and for v' we have taken a value corresponding to a turbulent intensity such that $v'/V = 20\%$, found as a realistic value by Pretrel [3].

- The vaporization requires further investigations, therefore a specific balance has been written. Introducing the water vapor amount $Y(z)$ (in kg of water per kg of dry air), we consider its variation along the path dz. This is a one dimensional modeling. The difference between $Y(z)$ and $Y(z+dz)$ is due to the vaporization of droplets inside the area between z and $z+dz$:

$$\rho.V.\frac{\partial Y(z)}{\partial z} = N_d.m_{ev} \tag{9}$$

  where N_d is the number of droplets per cubic meter inside the volume which is of interest and m_{ev} is the weight of evaporated water per second for a single droplet, which is modeled in a simple manner as suggested by Sirignano [14]:

$$m_{ev} = 2.\pi.d.\rho.\mathcal{D}.ln(1+B_M) \tag{10}$$

  where d is the diameter of the droplet, $\mathcal{D}$ is the mass diffusion coefficient of water vapor in air and where

B_M is the Spalding number defined as:

$$B_M = \frac{Y_{\text{sat}} - Y(z)}{1 - Y_{\text{sat}}} \tag{11}$$

Y_{sat} is the corresponding asymptotic value of $Y(z)$, at the same temperature, but when the air is saturated with water. The evaluation is performed on a mean Sauter diameter and extrapolated to the whole medium, considering the equivalent number of mean droplets that would correspond to the exact amount of liquid phase in the spray. This is an approximation, though yielding an estimation for the vaporization rate and the way it will affect the heat transfer (note in particular that the Sauter diameter is defined as the ratio between the volume of the droplet phase and the exchange area between the droplets and the gas phase, two main characteristics in the vaporization process). The moisture is then introduced in the computation of the wet air radiative properties to take into account the modulation of the water vapor rate due to droplet vaporization.

In the energy balance, the heat exchange due to vaporization is simply given by:

$$\dot{Q} = -N_d.m_{ev}.L_v \tag{12}$$

2.3 RTE formulation

The so-called RTE expresses the variation of the intensity along the path ds as a competition between various phenomena which enforce or decrease the intensity. The following formulation features, at the right hand side, decrease due to absorption by droplets and by gases, decrease by scattering due to the droplets, increase by emission due to both phases and finally increase due to scattering of all radiations in direction $\vec{\Omega}$:

$$\frac{\partial I_\lambda(s,\vec{\Omega})}{\partial s} = -\left(\kappa_{d\lambda} + \kappa_{c\lambda} + \sigma_{d\lambda}\right).I_\lambda(s,\vec{\Omega}) + \kappa_{d\lambda}.I^0_\lambda(T_d(s)) + \kappa_{c\lambda}.I^0_\lambda(T_c(s)) + \frac{1}{4\pi}\int_{\Omega'=4\pi} \sigma_{d\lambda}.P_\lambda(\vec{\Omega}' \to \vec{\Omega}).I_\lambda(s,\vec{\Omega}').d\Omega' \tag{13}$$

The coupling problem lies in the introduction of the intensity and the temperature, both involved in the energy balance and in the RTE. Here again the assumption of equal temperature for the two phases will be supposed to be valid.

The relevant radiative properties are $\kappa_{c\lambda}$, $\kappa_{d\lambda}$, $\sigma_{d\lambda}$, $P_\lambda(\vec{\Omega}' \to \vec{\Omega})$, respectively corresponding to the gas and droplet spectral absorption coefficients, the droplet spectral scattering coefficient and the spectral scattering phase function of the medium. The present formulation considers that the absorption phenomena may be simply

added without any more complex combinations. The radiative properties of the droplets are computed from the Mie theory. Main formulation may be summarized as follows:

- *spectral absorption coefficient*

$$\kappa_{d\lambda} = \int_0^\infty \pi.r^2.Q_{a\lambda}(r).N(r).dr \tag{14}$$

- *spectral scattering coefficient*

$$\sigma_{d\lambda} = \int_0^\infty \pi.r^2.Q_{s\lambda}(r).N(r).dr \tag{15}$$

- *spectral scattering phase function*

$$P_\lambda(\theta) = \frac{1}{\sigma_\lambda} \int_0^\infty \pi.r^2.Q_{s\lambda}.P_\lambda(r,\theta).N(r).dr \tag{16}$$

where $N(r).dr$ is the number of droplets having a radius between r and $r + dr$ per cubic meter. The detailed formulation and the numerical computation of the involved variables (absorption and scattering efficiencies ($Q_{a\lambda}$ and $Q_{s\lambda}$) and the scattering phase function for a given droplet size in a given direction ($P_\lambda(r,\theta)$)) are given in Berour *et al* [10] and are not recalled here.

Note that a renormalization process is applied on the scattering phase function, in order to avoid any non-conservation in the radiative transfer balance, potentially introduced by the discretization scheme imposed by the Discrete Ordinates Method processing.

The continuous phase only absorbs radiation, but this is not a simple problem to address, considering the strong non-gray behavior of carbon dioxide and water vapor. This difficulty is addressed using a correlated-K (so-called c-K) model aimed at the computation of the absorption coefficients of the gas phase. The formulation by Soufiani and Taine [15] has been introduced. A seven point Gaussian quadrature scheme has been applied and the database of reference [15] has been used for all the required spectral parameters aimed at the characterization of H_2O and CO_2 mixtures. The 43 band c-K model with irregular band widths has been chosen, since it yields a very good compromise between computation time and spectral accuracy. Once the seven quadrature points κ_j are known on each band as an accurate representation of the vapor phase absorption coefficients, the RTE is rewritten in the form:

$$\frac{\partial I_j(s,\vec{\Omega})}{\partial s} + (\kappa_{d\lambda} + \kappa_j + \sigma_{d\lambda}) .I_j(s,\vec{\Omega}) = (\kappa_{d\lambda} + \kappa_j) .I^0_\lambda(T(s)) + \frac{1}{4\pi}\int_{\Omega'=4\pi} \sigma_{d\lambda}.P_\lambda(\vec{\Omega'} \rightarrow \vec{\Omega}).I_j(s,\vec{\Omega'}).d\Omega' \quad (17)$$

where I_j is a value corresponding to the j^{th} quadrature point.

The averaged spectral intensity on each of the 43 wavelength bands are finally computed as:

$$\overline{I_\lambda} = \sum_{j=1}^{7} w_j.I_j(s,\Omega) \quad (18)$$

where w_j is the weight of the j^{th} Gaussian quadrature point.

Note that a single additivity is supposed to be valid for the gas species properties (H_2O and CO_2) considering the fact that carbon dioxide is involved at very low volume fractions.

The work has been specifically aimed at the treatment of the radiative transfer problem and has allowed the validation of the complete approach, involving radiative property computation, c-K model implementation and corresponding RTE solution.

2.4 Boundary conditions

Boundary conditions must be introduced for all balance equations.

- For the radiative part of the problem, all boundaries are supposed to be transparent (owing to the low volume fraction of droplets, this is a correct assumption); the incoming radiation is supposed to correspond to a blackbody intensity (at surrounding temperature for the upper boundary and the side opposite to the flame, at outlet temperature for the outflow section of the spray and at the characteristic flame temperature at the fire side).

- Thermal boundary conditions have to represent the heat exchanges between the computational domain and the surrounding medium. A Dirichlet condition is set at the upper boundary (where droplets and air are introduced). The flow is supposed to be thermally developed at the outflow, which leads to a zero normal derivative for the temperature at the bottom of the curtain. Fourier's conditions are imposed at the other boundaries (with an arbitrary value for the convection coefficient). Such conditions could be discussed if an actual influence of the bottom boundary condition or of the convection coefficient value was observed. However, as will be mentioned in the result section, the temperature everywhere in the spray remains close to the surrounding one, with no strong temperature gradients potentially affected by a boundary condition choice.

- Finally the moisture is computed from given conditions at the inlet (the relative moisture is fixed for the incoming air), whereas the flow is supposed to be fully developed at the outflow (leading to a zero derivative). The balance for the moisture is one dimensional avoiding the need for boundary conditions at the lateral sides of the domain.

3 Numerical procedures

An iterative scheme is applied to deal with the coupling problem. Figure 2 shows a schematic description of the used algorithm. A preprocessing step yields the radiative properties in a database, which is stored once and for all, on the basis of input data (namely the temperature and volume fraction ranges, the droplet size distribution, the directions fixed by the quadrature scheme). Considering the temperature and moisture field evolutions, the radiative properties for the gas phase will be updated after each loop, taking into account the actual H_2O and CO_2 volume fractions (or if necessary temperatures).

Starting with an initial field at surrounding conditions, a solution is sought for the RTE, then the corresponding radiative flux divergence will be introduced in the energy balance, together with the calculated moisture distribution. The RTE is in fact solved until the normalized residuals between two successive solutions on the intensity and summed over each grid node, each direction and each wavelength is found less than 10^{-10}. The solution for the temperature is then computed for the whole domain and will be re-introduced in the RTE for a second loop. Successive iterations are performed until a given convergence criterion is satisfied (here again when the sum of the normalized residuals between two successive iterations, for the temperature this time, is found less than 10^{-10}). Typical results presented in the following paragraphs have been obtained, stopping the computations after 10 to 25 complete loops (RTE + energy balance), depending on the coupling level.

[Figure 2 about here.]

3.1 Finite volume scheme

The finite volume method has been chosen for the solution of the energy balance, since the present work is planned to be combined with a solution for the dynamics of the problem, which is classically well solved applying a SIMPLE algorithm-like scheme. The adaptation of the method to the solution for the temperature distribution follows the proposal by Patankar [16]. All details of the formulation may be found in this reference.

Nevertheless some numerical choices have been made to ensure the convergence of our results, which can be specified here. This mainly concerns two points : the way in which the competing effects of diffusion and convection are treated and how the linearization of the source term is introduced (bearing in mind that radiative transfer will be a dominant exchange mode, thus able to make the numerical process unstable if inadequately treated as a source term).

First of all, when conduction and convection are involved in the same equation, one of the two terms may prevail over the other. That is why a numerical scheme has to be carefully chosen to avoid any problem of numerical diffusion. Among the existing schemes (upwind scheme, power law, hybrid scheme, quick scheme, ...) we adopted the power law scheme, because of the best compromise that it offers between the calculation speed (without the computation of exponential terms) and the result accuracy.

Afterward, application of the finite volume method will provide a system of equations which will be presented in a matrix form. In order to ensure the convergence of the solution, some mathematical properties must be satisfied which, without recalling all the conditions, require the source terms to be linearized. This is the second difficulty addressed in this paragraph and the general method suggested by Patankar [16] is followed. For a given source term S, this implies after a Taylor development that:

$$S \approx S^* + \left(\frac{\partial S}{\partial T}\right)^* \cdot (T(s) - T^*(s)) \tag{19}$$

where the terms marked with the superscript $*$ are taken at the previous iteration. The second term on the right hand side can be considered as a correction between the two iterations that will vanish as convergence on the temperature distribution is achieved.

The radiative source term is treated after being integrated on a cell with dimensions $\Delta y.\Delta z$, which corresponds to

$$S = -\vec{\nabla}.\vec{q}_r.\Delta y.\Delta z \tag{20}$$

Considering equation (5), only the part of the radiative flux divergence that involves the black body intensity exhibits an explicit dependence in T. Consequently the derivative of the source term will be reduced to

$$\left(\frac{\partial S}{\partial T}\right)^* = -\int_{\lambda=0}^{\infty} \kappa_\lambda.4\pi.n_\lambda^2.\frac{\partial I_\lambda^0(T(s))}{\partial T}.d\lambda.\Delta y.\Delta z \tag{21}$$

This of course avoids the implicit dependence of the medium intensity in the temperature through the emission

term, but as convergence will be achieved, S will finally be equal to S^*, a source term computed with the exact formulation according to relation (5).

Considering the blackbody intensity defined by:

$$I_\lambda^0(T(s)) = \frac{C_1}{\lambda^5.\left(exp\left(\frac{C_2}{\lambda.T(s)}\right)-1\right)} \tag{22}$$

with $C_1 = 1.19088\text{x}10^{-16}\ W.m^2.sr^{-1}$ et $C_2 = 0.014388\ m.K$

This implies:

$$\frac{\partial I_\lambda^0(T(s))}{\partial T} = \frac{C_2.C_1.exp\left(\frac{C_2}{\lambda.T(s)}\right)}{\lambda^6.\left(exp\left(\frac{C_2}{\lambda.T(s)}\right)-1\right)^2.(T(s))^2} \tag{23}$$

which allows the introduction of S in a linearized form. The resulting numerical scheme is stable.

Note that the other source terms do not introduce any supplementary difficulty since the conduction and turbulent diffusion terms are functions of the temperature gradient and are therefore handled in a straightforward manner, whereas the vaporization source term is assumed constant in the cell (it does not depend directly on the temperature), thus avoiding any possibility of instability consequence.

3.2 Discrete Ordinates Method

Only the main features of the numerical processing will be given here, since the applied scheme has been extensively detailed in Berour *et al.* [10] and in Lacroix *et al.* [17]. Let us just recall here that equation (17) is treated in a straightforward manner (instead of dealing with the integrated form of the RTE as it is sometimes done). Renormalization of the scattering phase function and introduction of a fine spectral treatment are the two precautions taken before solving the RTE numerically, for a sake of accuracy. In a classical manner sweeping of the computational domain is performed starting from each corner using a first order scheme and in accordance with the known boundary conditions.

When addressing the complete 2D problem, the angular discretization is performed using a $DCT111$ quadrature (see Koch *et al.* [18] for the definition of the corresponding direction cosines) and the closure scheme is the one by Carlson and Lathrop [19]. A coarse regular grid of 80x30 nodes has been observed to be sufficient in the typical cases hereafter discussed. Accuracy of the results has been checked to verify the independence of our numerical prediction from the mesh, the quadrature scheme and the closure relations.

4 Numerical results

In relation to the assumptions discussed at the beginning of the formulation section, dynamic characteristics used as input data in the following test cases will be first specified. They are taken from a review of experimental data by Pretrel [3], Dembélé [4] and Zimmer [11]. This allows a complete computation of the problem where radiative transfer is combined with the other energy exchange modes. Let us specify that in the subsection devoted to the validation, only the radiative transfer problem is addressed, so that the droplet size distribution and the spray dimensions are the only input data required.

- the droplet size distributions are plotted on figures 3 and 4 for the two sprays studied hereafter, through the volume fraction corresponding to each diameter class (note that the diameter is ranging from 10 to 250 μm with a mean value around 100 μm; let us also mention that increasing the pressure for the droplet generation strongly rises the total number of droplets, an increase in the attenuation ability of the spray is therefore expected);
- the size of the spray (width x height) is 0.24 $m \times 2$ m;
- the velocity of the flow is constant and equal to 4.4 $m.s^{-1}$ for the spray referred as "TG03 - 1bar" and 2.6 $m.s^{-1}$ for the case "TG03 - 3bars" (as a result of an evaluation of the averaged velocity taking into account the spray dimensions and the liquid flow rate);
- the turbulence intensity is fixed to 20%;
- surrounding air characteristics are 300 K and 50% relative humidity;
- the volume fraction of water vapor in air (f_{H_2O}) is easily deduced from the moisture $Y(z)$ (which is computed as explained in paragraph 2.2) using the molar weights of water and air for example; the corresponding amount of CO_2 is thereafter calculated as suggested in [3]: $f_{CO_2} = 0.0003 \cdot (1 - f_{H_2O})$.

Supplementary numerical conditions are required for the thermal characteristics. The radiative source is a black body at high temperature. Assuming some distance between the radiative source and the target itself, the radiative flux received by the spray is set to a realistic power level of 50 kW/m^2 when diffuse irradiation is considered, as a rough value suggested in [3]. Finally, the convection coefficients aimed at the modeling of the heat exchange with the surrounding medium (used for the application of Fourier's conditions) are set to 10 $W.m^{-2}.K^{-1}$.

[Figure 3 about here.]

[Figure 4 about here.]

4.1 Validation

Considering the major role expected for the radiative transfer in our computations, the first test case is a simulation of experiments carried out under laboratory conditions and reported in [4], in which the phenomenon of radiative transfer is studied exclusively. This test has been chosen since complete information is available on the features of the spray (presented in Figure 3 and 4) and because results concern spectral normal transmissivity measurements, detailed information easy to achieve with our code (calculating the ratio between the intensity at $y = 0$ in the y direction and the incident radiation at $y = L$). Experimental conditions correspond to a collimated irradiation on a spray. Consequently, a limited incident energy is induced, the temperature is supposed to be little affected by radiation absorption and the treatment of radiative transfer can be uncoupled from the rest of the problem, assuming constant moisture and temperature. Following [4] the relative moisture and the temperature inside the spray are therefore not computed but rather set to 60% and 300 K. In these conditions, the problem may be simplified to a one dimensional configuration with azimuthal symmetry. This leads to a huge reduction of the required computational resources and allows the discretization to be refined according to the polar angle, which is needed owing to the strong directional variations that are expected. Hence a small regular step of 0.5 degrees is used in order to ensure an accurate treatment of the scattering effects. Corresponding results presented on Figure 5 confirm the capability of our model to predict the radiation attenuation due to the spray. The transmissivity is plotted as a function of wavelength, in the range corresponding to the main part of the incident energy for the two typical sprays previously described. Comparisons may be carried out with the experimental curves, which have been re-drawn according to [4]. The spectral variations are reproduced and the averaged transmissivity level is also correctly captured. In particular, the c-K model accurately deals with well-defined spectral peaks due to H_2O and CO_2, whereas scattering and absorption phenomena due to the droplets are responsible for the global attenuation and are also correctly dealt with. At first sight the intensity of the various peaks may seem to be miscalculated, but this can be explained by a spectral resolution which was finer in the experimental data (25 cm^{-1}), while the band width is varying in the present numerical study from 25 to 100 cm^{-1} according to the spectral discretization suggested in [15]. Since the results of the present study yield a mean value for each spectral band, the integral over the whole spectral range gives a correct estimation

of the total transmissivity (92% compared to a reported experimental value of 90% in the "1 bar" case and 82.1% compared to a reported experimental value of 81.4% in the "3 bars" case). Owing to a larger droplet density number and also to a slightly smaller mean droplet diameter, the so-called "TG03 - 3 bars" has a better attenuation ability and the present model reproduces this trend very well.

[Figure 5 about here.]

The radiative part of our numerical code being now validated in conditions where the directional variations are very crucial, the next paragraphs will deal with complete simulations of the combined heat transfer, where diffuse radiation is considered and hemispherical transmissivities are studied. Consequently the directional variations of the intensity will be less strong. On the contrary temperature and moisture distributions will vary with the spatial co-ordinates, which will not allow the assumption of a one dimensional problem with azimuthal symmetry. Consequently a classical quadrature for all the directions of the whole space will be used: this is the $DCT111$ scheme as discussed in paragraph 3.2, which has been validated in a particular study exclusively devoted to the radiative problem.

4.2 Water spray curtain characterization

The first configuration which is presented here concerns the "TG03 - 3 bars" case when one single spray is considered, addressing the whole problem of coupled heat transfer (next tests will mainly deal with the "TG03 - 3 bars" case which was observed to yield the strongest attenuation, but various nozzle combinations will be studied). Figure 6 is a map of the temperature distribution which has been predicted considering diffuse irradiation. Isotherms are presented with temperatures indicated in Kelvin. The flame is radiating from the right hand side and droplets are falling from the top, inducing an air flow due to drag effects. The temperature which is 300 K at the top of the domain is seen to increase progressively due to radiation absorption and reaches a maximum value around 305 K at the bottom corner of the flame side. Despite the strong irradiation (as indicated 50 kW/m^2), the rise in temperature is therefore weak, due to compensating effects that will be discussed later.

Figure 7 is a complementary description of the spray properties devoted to the moisture evolution. The amount of moisture in air (in g of water / kg of air) is plotted as a function of the space co-ordinates using isolines, just as for the temperature in the previous figure. Due to vaporization process, the amount of water in the air is seen to increase progressively as the droplets are falling. The moisture consequently rises from its initial value

at the inlet (11.2 g of water / kg of air) to reach the maximum value of 17 g of water / kg of air. Owing to the fact that the temperature also rises, this yields a relative humidity which actually increases (varying between 50% to 60% at the bottom of the spray). In any case these variations, obtained for temperature and moisture with a complete treatment of the balance equations, yield realistic distributions. On the contrary, assumptions like those used in the validation section, where the conditions were 300 K and 60% of relative moisture, imply a constant amount of water equal to 13.4 g / kg of air. Compared to the map of Figure 7, this seems to be a correct mean value, even if local discrepancies are observed, which could affect the attenuation peaks due to the continuous phase. This will be further discussed at the end of the present section for various configurations. Note also that the increase of vapor in air corresponds to an average loss in size of around 10% for the droplets. The assumption of constant droplet diameters is consequently not exactly valid, but not so far from reality either.

At this stage, values introduced for the incoming radiative flux and the heat transfer coefficient at boundaries may be also discussed. As can be stated, despite the strong radiative source and even at the flame side, actual spray temperature does not change much from surrounding conditions (an increase in the convection coefficient would even enforce this trend). Moreover, the discrepancy with the high temperature level of the radiative source is obvious and a modification of the above entry data would not affect the present results sufficiently to change this. Slight modifications of these values would not bring complementary information for us at this stage of simulation where dynamics would have first to be improved before refining the analysis.

[Figure 6 about here.]

[Figure 7 about here.]

Phenomena involved in the energy exchanges may be evaluated considering the role of the various transfer modes which have been identified in paragraph 2. Figure 8 presents the contribution to heat transfer due to the diffusion phenomena (top left Figure), the convection due to the droplets and air (top right Figure), the vaporization (bottom left Figure) and finally to the radiative transfer (bottom right Figure). All data are presented as power densities (in kW/m^3) in order to allow the comparison of their respective part. At every position in the domain a summation of the various contributions would yield zero, as a result of the competing transfer phenomena. The contribution called "diffusion" corresponds to the divergence of the sum $(\vec{q}_k + \vec{q}_t)$, the "convection" is the result of relation (2) (with a minus sign in order to put all terms involved in balance

(1) at the right hand side), the "vaporization" is the result of equation (12) which features the heat loss due to vaporization and finally the "radiative transfer" is the result of equation (5) corresponding to the divergence of the radiative flux. As can be seen, radiative transfer induces a strong heat source, which is essentially balanced by convection and vaporization, whereas diffusion effects are less important (except in the bottom right corner where the temperature is the highest), inducing an homogenization of the distributions in the y direction however. Vaporization effect is seen to be really crucial in determining the energy balance, due to the previously observed increase of water vapor in air combined with a large value of the latent heat. Note that the isolines featuring the power density due to radiative transfer and vaporization have a similar pattern, with the strongest contributions located at the bottom right corner of the domain (corresponding to the bottom of the curtain at the fire side). On the contrary convection and diffusion have different patterns as a consequence of their modeling which is one dimensional (according to the z direction for the convection and to the y direction for the diffusion).

[Figure 8 about here.]

In the present case, the spectral transmissivity has been also plotted as a function of the vertical position at the side opposite to the flame. The ratio of the flux at $y = 0$ divided by the incident flux at the flame side has been calculated to yield an hemispherical transmissivity. The map presented on Figure 9 shows how the transmissivity level varies with the wavelength as a consequence of sharp variations in the attenuation due to the gas phase. The mean behavior is similar to the curve presented in the validation section (see Figure 5). The level is slightly higher since hemispherical transmissivity is considered here, instead of a directional value. Effects due to the 2D treatment of the problem may be also observed since transmissivity levels, also plotted as a function of the vertical position, decrease near the top and bottom boundaries. Actually the transmissivity really reaches a constant value at positions around 0.5 m from the limits of the computational domain. Of course this holds for diffuse rather than collimated irradiation and is mainly due to geometrical rather than to physical reasons (part of the radiation is lost through the top and bottom faces of the domain) but scattering can enhance the phenomenon. This also illustrates the discrepancy in prediction when introducing the real dimensions of the device (in particular the height) instead of simply considering a one dimensional analysis as if the height of the curtain was infinite.

[Figure 9 about here.]

Let us now try to improve the attenuation ability of the water curtain, combining several nozzles in order to increase the optical depth of the spray. We suppose that the size distribution plotted on Figure 4 keeps the same shape and is only multiplied by a constant factor as a function of the nozzle density. A first solution is to associate the nozzles in "parallel", keeping the same width for the spray. As an example, Figure 10 and 11 concern the prediction of temperature and moisture computed for 4 nozzles, yielding a nozzle density of 16.6 sprays per meter, whereas the previous cases was corresponding to a value of 4.2 sprays per meter (since the width and the thickness of an individual spray is 0.24 m). As can be seen, due to an increase in the droplet density, radiation absorption involves a higher temperature level (with a maximum value around 307 K). As in the previous case, this increase is limited by the vaporization process all the more because the number of injected droplets is larger. Consequently, the maximum amount of water vapor in air rises until 27 g / kg of air. The intensity of the attenuation peaks due to the continuous phase can be affected by these conditions, which begin to be difficult to predict without a combined treatment of energy and radiative transfer. This is illustrated on Figure 12 where the transmissivity is plotted at the side opposite to the flame. In comparison with Figure 9, the transmission of radiation is seen to be notably reduced, except in the short wavelengths. The global attenuation is increased since droplets and vapor lead to a larger resulting optical depth. Information on the transmission level at a mean vertical position in this plane will be also given later in a summary figure allowing a comparizon in various spray configurations with predictions obtained when the radiative problem is addressed uncoupled from the other transfer modes.

[Figure 10 about here.]

[Figure 11 about here.]

[Figure 12 about here.]

To continue the comparison with the case where a single spray is considered, one can plot the contribution of the involved transfer phenomena as in Figure 8. This is done with the same notations in Figure 13. What is obvious is the increase in the power densities involved in the energy balance and especially in what concerns the two major contributions due to radiative transfer (as an energy source) and the vaporization (as an energy loss). Another peculiar feature is the change in sign in the convection contribution. As can be seen at the top of the spray, the convection first induces an energy source and then an energy loss down in the domain. Here again, the reason is the vaporization which induces a cooling of the flow just after the inlet, before that the radiation

absorption results in an increase of the temperature. This is confirmed on Figure 10 where an isotherm around 299 K is seen at the top of the domain illustrating that the heat loss is not yet overwhelmed by the radiation effects at this location. Such a temperature level below the entry temperature (300 K) may seem surprising at first glance but can be explained numerically. Vaporization is here mainly due to a moisture gradient between driven air (50% of relative moisture) and droplet surface (saturated in moisture). The phase change results in a cooling of the medium and induces a slight temperature decrease.

[Figure 13 about here.]

One can compare this configuration of device "in parallel" with the case where the sprays are associated "in series" in order to enhance the spray width, whereas the nozzle density (in spray per meter) is the same as in the first test case that was presented through Figure 6 to 9 (4.2 sprays per meter). The resulting temperature and moisture fields are given on Figures 14 and 15. Isolines are plotted for the whole domain with dimensions now equal to 2×0.96 m. The highest levels reached in the spray are close to those observed with the single spray (maximum values around 303 K and 16.5 g of water / kg of air). However, due to a larger width, the vaporization now induces a decrease in the temperature which is not balanced by the radiation absorption at the side opposite to the flame, where the temperature decreases to 298.7 K. The contributions to the energy balance are very similar to those presented on Figure 8, with the same maximum levels and similar patterns (they are consequently not represented here). Just notice that the vaporization overwhelms the radiative transfer at the left bottom corner of the domain, as explained above. The resulting transmissivity is presented on Figure 16. The attenuation is now stronger in comparison with the previous cases due to the fact that the curtain width is four times greater. This is true even when compared with the simulation of four sprays "in parallel", which is interesting owing to the fact that the same number of sprays and consequently the same liquid flow rate are used in the present case. The resulting total transmissivity, integrated on the wavelength range is 49.6% (in comparison with the value 85.3% for the single spray and 66.5% for the device "in parallel"). However, the view factor for two semi-infinite planes, 2 m in height, separated by a distance of 0.72 m (the difference between the widths 0.24 m and 0.96 m) is around 0.70. Correcting curve 3 with this factor would produce a transmissivity very close (and even smaller) to the level of curve 4. Consequently the device of sprays "in parallel" would seem slightly better. What is also visible, is that the transmission level is no more constant as a function of the height, even around the mean vertical position. The present 2D analysis predicts a minimum attenuation at the central position, which immediately increases toward the top and the bottom of the domain. Apart from

the position $z = 1\ m$, the device of sprays "in series" would therefore seem to be the best. Globally the two solutions "parallel" and "series" are indeed very close to each other.

[Figure 14 about here.]

[Figure 15 about here.]

[Figure 16 about here.]

In order to summarize the previous radiative results, the predicted transmissivities numerically computed in the above-discussed cases are now plotted on the same figure (Figure 17). The spectral transmission level obtained at the mean vertical position given by $z = 1\ m$ is presented as a function of the wavelength with continuous lines. They are also compared with the values that would be obtained addressing the radiative problem uncoupled from the rest of the energy transfer, as in the validation section with the following characteristics: 60% of relative moisture and 300 K (dotted lines). The above analysis has shown how the temperature and the moisture are affected due to combined energy transfer phenomena. Figure 17 shows that it induces a slight modification of the transmissivity around the peaks due to H_2O and in the largest wavelengths, whereas the short wavelength range can be correctly treated with an uncoupled radiative model (provided that we are able to introduce realistic data for the temperature and the moisture, which can be sometimes difficult without modeling those characteristics). Actually, the role of water vapor in the continuous phase explains this correction. Note that strong variations along the vertical position had been observed in the previous transmission figures and the present comparison is only valid at the mean vertical position. The discrepancy would be larger near the top or the bottom of the curtain. Moreover a single radiative analysis, would not allow us to understand the complex energy exchanges due to the various transfer phenomena and in particular the role of the vaporization.
Concerning the curtain characterization, the role of the spray device seems to be obvious, comparing curves 3 and 4, confirming an apparent stronger attenuation when sprays are added in "series". However, as discussed above, considering the difference in width and a correction applying a view factor to take it into account, the two solutions are indeed equivalent. Finally the role of the droplet concentration also appears through the comparison between the basic case "single spray" of the "TG03 - 3 bars" (curve 2) and the simulations 3 and 4 where the attenuation of radiation is clearly enhanced, with a droplet density risen by a factor 4.

[Figure 17 about here.]

5 Concluding remarks and future works

The present work has allowed the prediction of the radiation transmission through a given water curtain. Test cases of sprays used as thermal shields located near the target to be protected (relatively far from the fire), exposed to a strong radiative source on one side, have been simulated. Different sprays have been considered owing to the available knowledge of the parameters characterizing them, which has allowed an extensive study of their behavior. Following items summarize the results.

- The coupling between the energy balance and the RTE has indicated strong competing phenomena. Radiative heat source is balanced by heat losses due to convection and vaporization. This results in temperature levels inside the medium close to the surrounding conditions despite strong irradiation.

- The role of droplets in governing the global attenuation has been confirmed, whereas water vapor has been observed to yield absorption patterns in definite bands.

- Droplet volume fraction increase results in transmissivity decrease, the lowest value of transmissivity integrated over the whole wavelength range being below 50% (when considering a heat source with an incident radiative flux set to $50 kW/m^2$, and a nozzle density of 16.6 nozzles/m with nozzles of the so-called TG03 type with a water pressure of 3 bars). Stronger attenuations could of course be predicted further increasing the nozzle density or the water flow rate.

- Combinations of nozzles in "parallel" (located side by side) or "series" (located one behind the other) have not been found to yield an actual modification of the attenuation ability.

- The radiative transfer problem can be treated uncoupled from the global heat transfer if a quick evaluation of the attenuation level is sought, providing realistic data for the temperature and the moisture. Such input data may be hazardous however and some inaccuracies will appear as wavelength increases. The role of the coupling is obvious when the droplet concentration is higher, since the transmissivity is affected by the amount of vapor in air, which rises due to vaporization.

- The present 2D configuration has shown that for problems with moderate dimensions, the radiation transmitted through the curtain toward the target may vary with the vertical position (perpendicular to the main radiation propagation direction). A 1D model will therefore be unable to capture such variations.

The present study has been carried out uncoupling the heat transfer from the dynamics, thus leading to as series of simplifying assumptions used for the representation of the spray flow. This drawback will be now avoided, associating a specific study of the dynamics of the spray to introduce more accurate data in the energy balance. The application to other nozzle types will be then considered, varying the droplet characteristics and the curtain geometries.

References

[1] T.S. Ravigurajan and M.R. Beltran. A model for attenuation of fire radiation through water droplets. *Fire Safety Journal*, 15:171–181, 1989.

[2] A. Coppalle, D. Nedelka, and B. Bauer. Fire protection : water curtains. *Fire Safety Journal*, 20:241–255, 1993.

[3] H. Pretrel. *Étude du comportement thermodynamique de pulvérisations liquides sous l'effet du rayonnement infrarouge. Application à la protection incendie par rideau d'eau.* PhD thesis, INSA de Lyon, 1997.

[4] S. Dembélé. *Modélisation et étude expérimentale des transferts de chaleur par rayonnement dans un rideau d'eau diphasique. Application à la protection incendie d'installations industrielles à risques.* PhD thesis, INSA de Lyon, 1998.

[5] S. Dembélé, A. Delmas, and J.F. Sacadura. A method for modelling the mitigation of hazardous fire thermal radiation by water spray curtains. *ASME J. Heat Transfer*, 119:746–753, 1997.

[6] S. Dembélé, J.X. Wen, and J.F. Sacadura. Analysis of the two-flux model for predicting water spray transmittance in fire protection application. *ASME J. Heat Transfer*, 122:183–186, 2000.

[7] G. Grant, J. Brenton, and D. Drysdale. Fire suppression by water sprays. *Progress in Energy and Combustion Science*, 26:79–130, 2000.

[8] J.F. Sacadura. Radiative heat transfer in fire safety science. *J. Quant. Spect. Rad. Tran.*, in press, 2004.

[9] W. Grosshandler, D. Lowe, K. Notarianni, and W. Rinkinen. *Protection of data processing equipment with fine water sprays.* NIST report, n° NISTIR 5514, 1994.

[10] N. Berour, D. Lacroix, P. Boulet, and G. Jeandel. Radiative and conductive heat transfer in a non-grey semitransparent medium - application to fire protection curtains. *J. Quant. Spect. Rad. Tran.*, 86:9–30, 2004.

[11] L. Zimmer. *Etude numérique et expérimentale de la turbulence en écoulement gaz-gouttelettes. Applications aux rideaux d'eau en présence de vent latéral.* PhD thesis, Institut Von Karman et UHP Nancy 1, 2001.

[12] J.F. Sacadura. *Initiation aux transferts thermiques.* Lavoisier Technique et Documentation, 1980.

[13] M. Rokni and B. Sunden. Numerical investigation of turbulent forced convection in ducts with rectangular and trapezoidal cross-section area by using different turbulence models. *Numerical Heat Transfer Part A*, 30:321–346, 1996.

[14] W.A. Sirignano. *Fluid dynamics and transport of droplets and sprays.* Cambridge University Press edition, 1999.

[15] A. Soufiani and J. Taine. High temperature gas radiative property parameters of statistical narrow-band model for H_2O, CO_2 and CO, and correlated-k model for H_2O and CO_2. *Int. J. Heat Mass Transfer*, 40(4):987–991, 1997.

[16] S.V. Patankar. *Numerical heat transfer and fluid flow.* Hemisphere Publishing Corporation, 1980.

[17] D. Lacroix, G. Parent, F. Asllanaj, and G. Jeandel. Coupled radiative and conductive heat transfer in a non-grey absorbing and emitting semitransparent media under collimated radiation. *J. Quant. Spect. Rad. Tran.*, 75:589–609, 2002.

[18] R. Koch, W. Krebs ans S. Wittig, and R. Viskanta. Discrete ordinates quadrature schemes for multidimensional radiative transfer. *J. Quant. Spect. Rad. Tran.*, 53(4):353–372, 1995.

[19] B.G. Carlson and K.D. Lathrop. Chap.3, transport theory - the method of discrete ordinates. In *Computing methods in reactors physics.* Gordon and Breach New York, 1968.

List of Figures

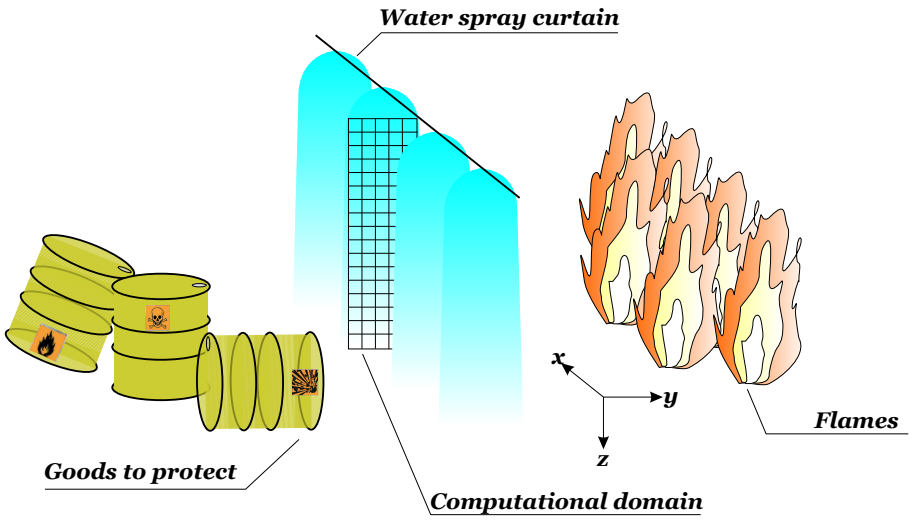

Figure 1: Problem description

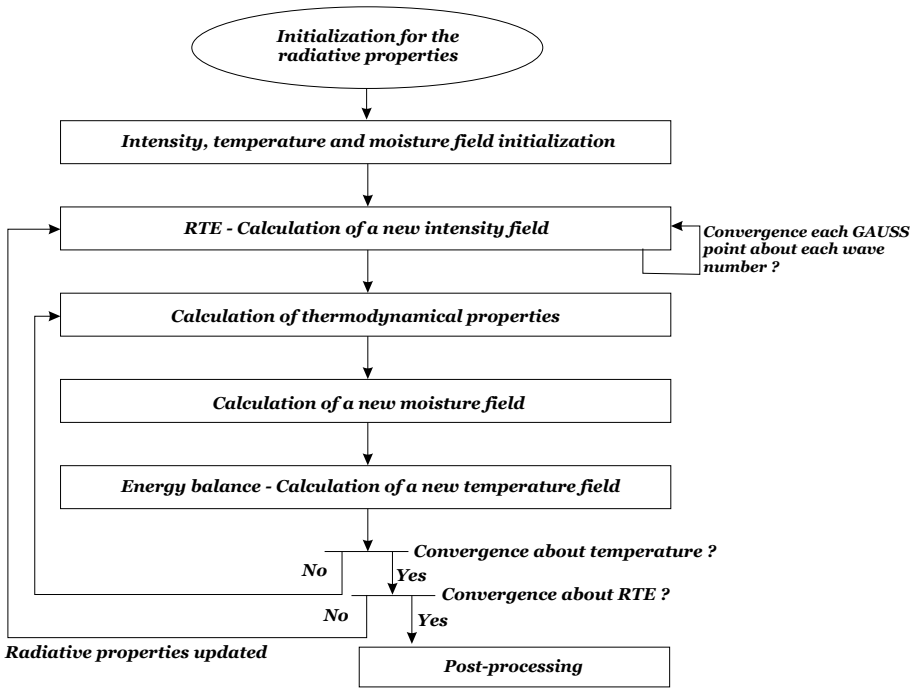

Figure 2: Schematic description of the numerical processing

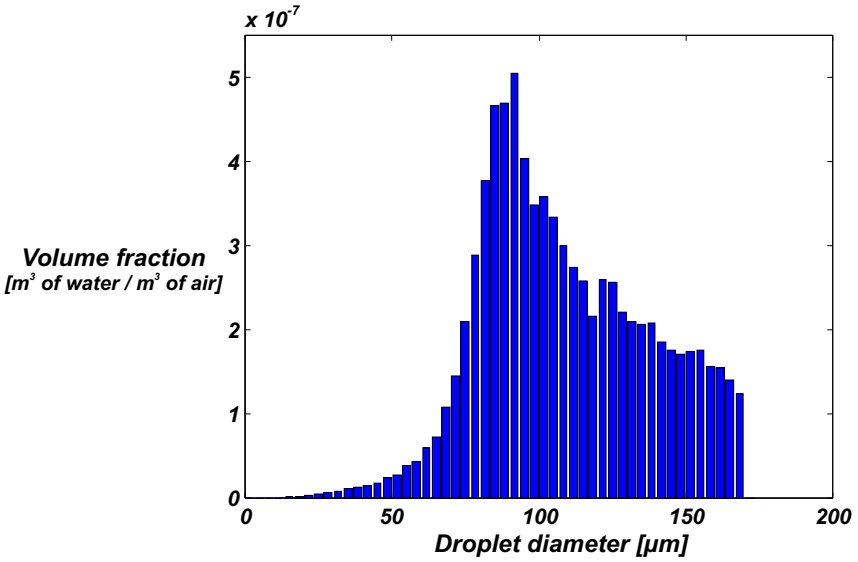

Figure 3: Size distribution used for the "TG03 - 1 bar" case according to [4]

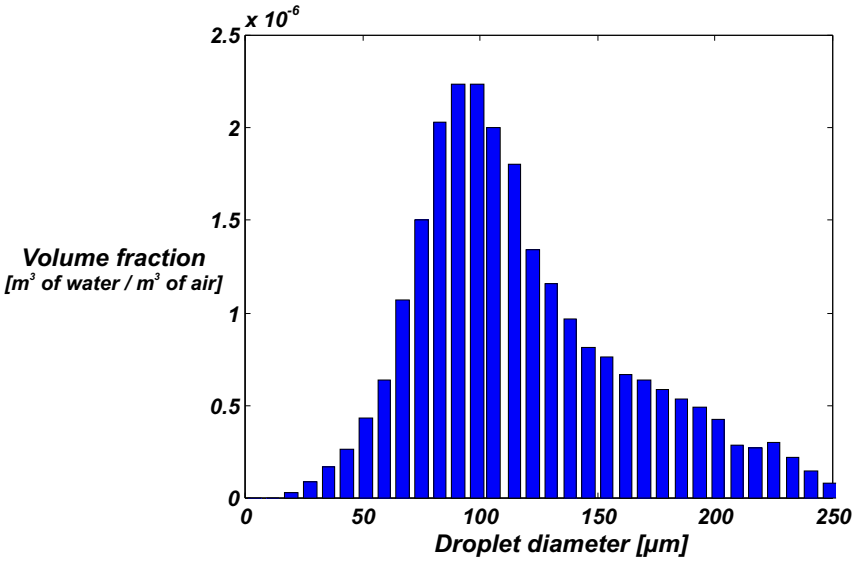

Figure 4: Size distribution used for the "TG03 - 3 bars" case according to [4]

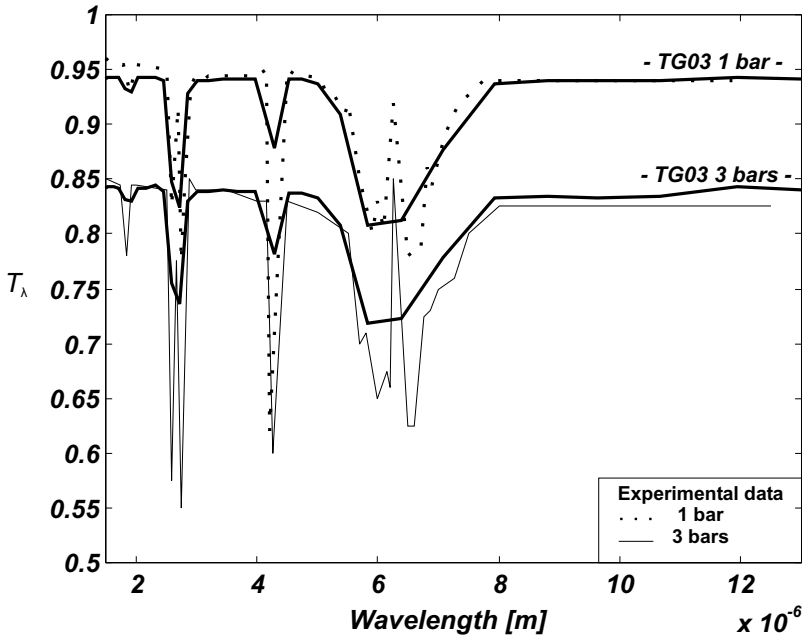

Figure 5: Spectral transmissivity predicted for a collimated irradiation. Comparison with the experimental data by Dembélé [4]

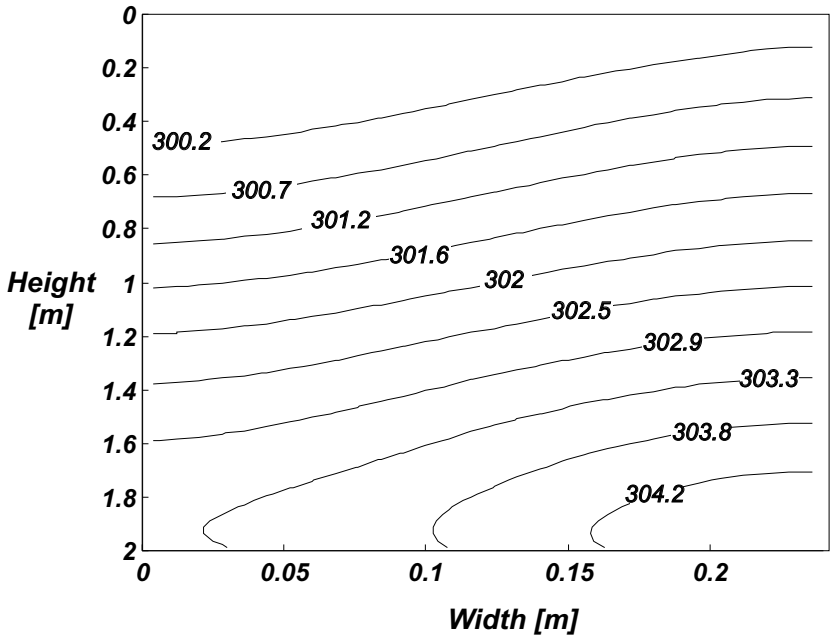

Figure 6: Predicted temperature field (in K) for the "TG03 - 3 bars" case (irradiation from the right side)

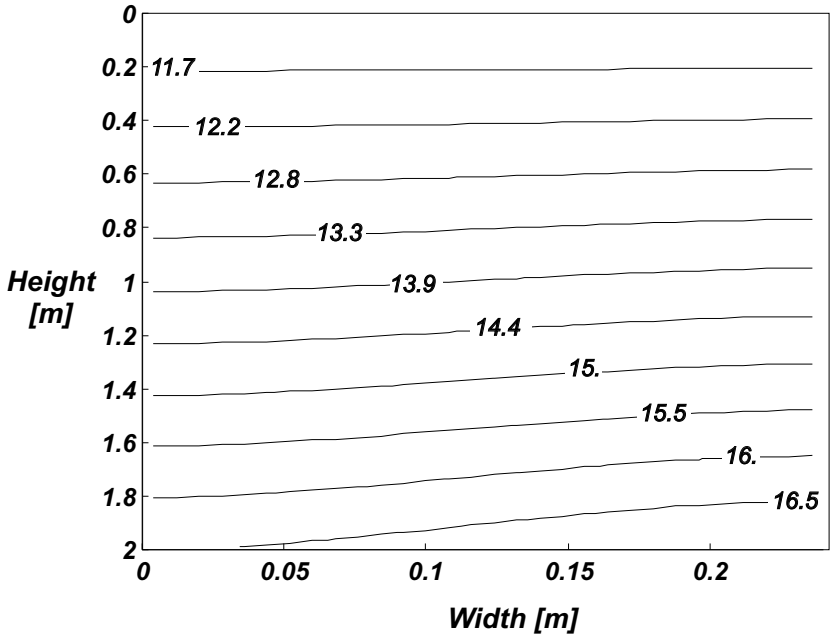

Figure 7: Predicted moisture field (in g of water / kg of air) for the "TG03 - 3 bars" case (irradiation from the right side)

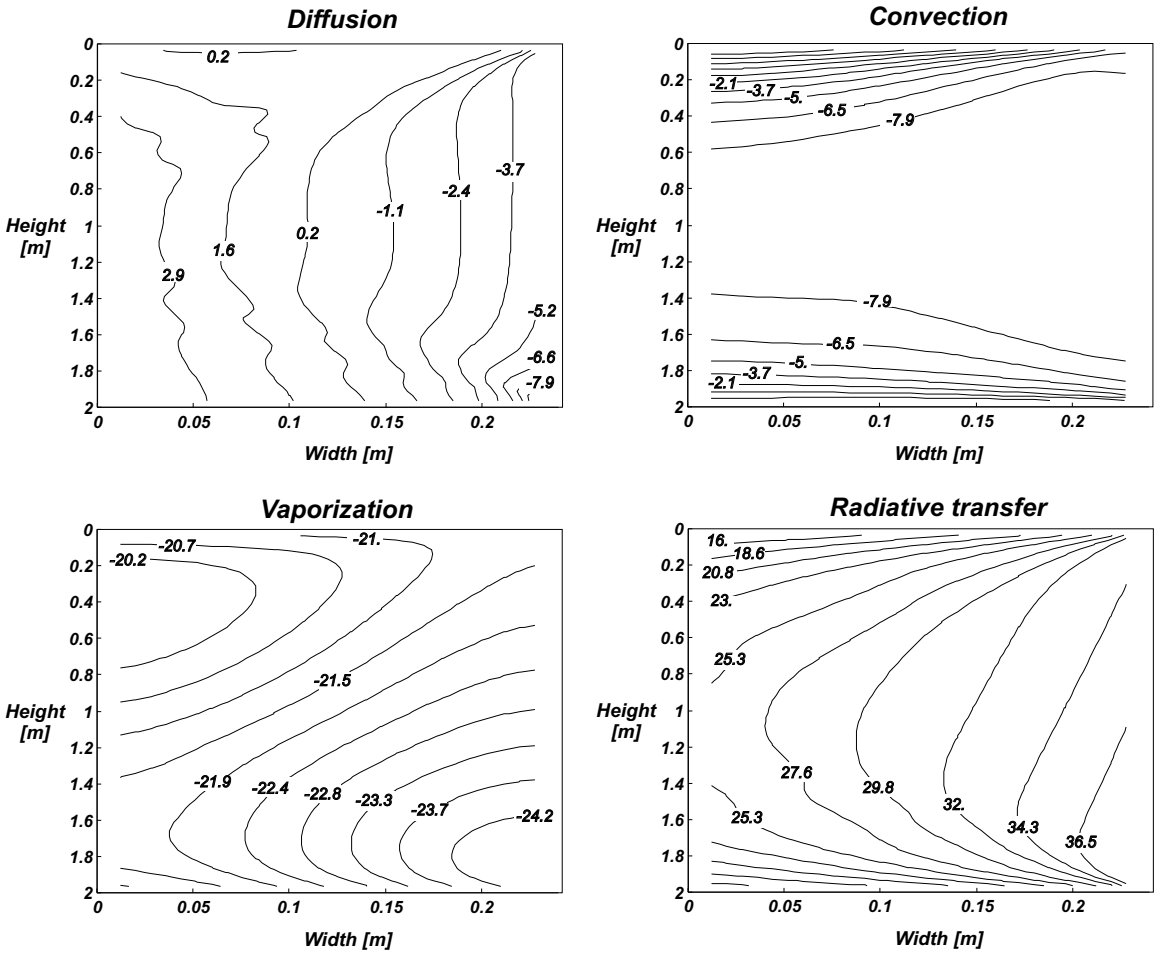

Figure 8: Contribution of the main transfer phenomena (in kW/m^3) for the "TG03 - 3 bars" case

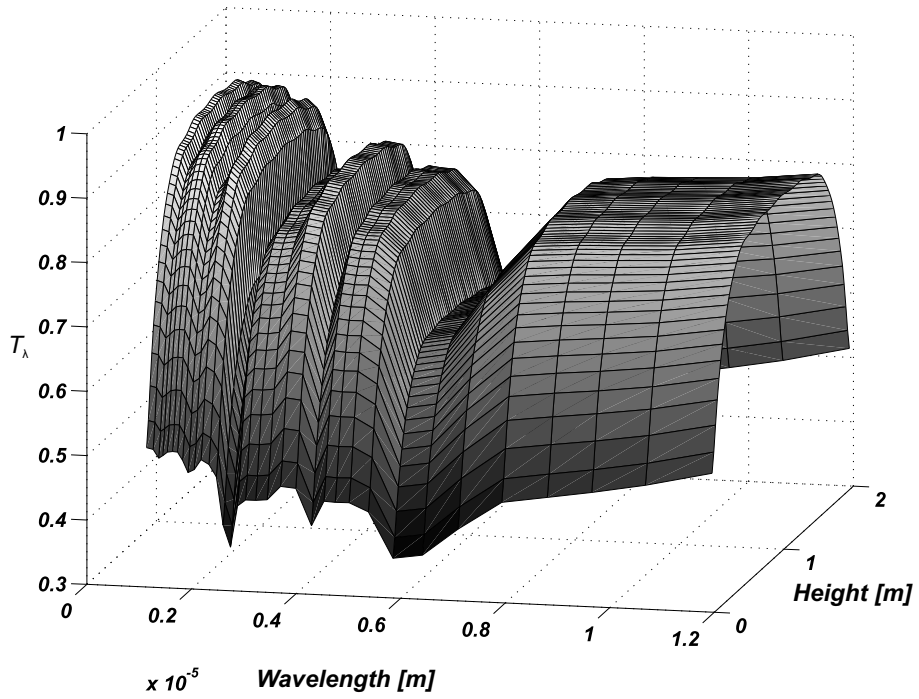

Figure 9: Spectral transmissivity in the plane opposite to the flame side ("TG03 - 3 bars" case)

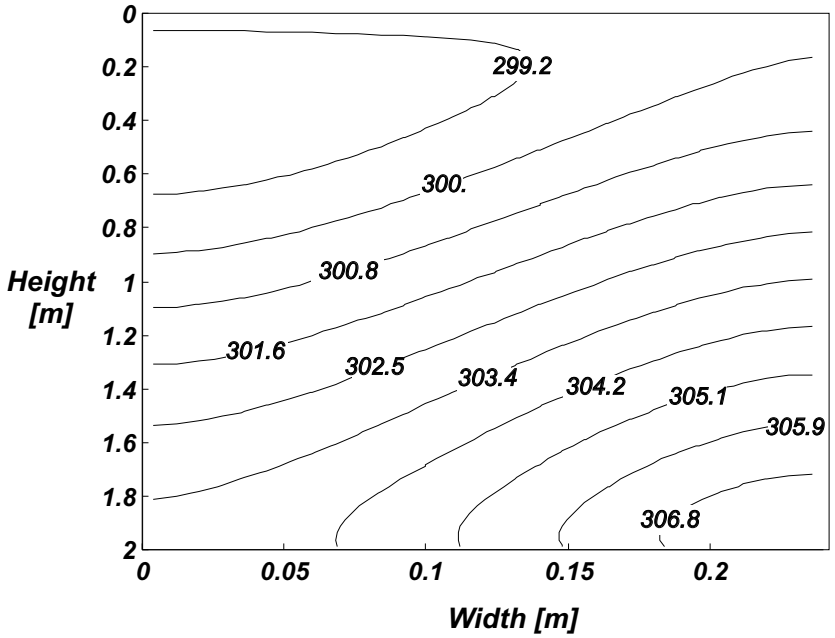

Figure 10: Predicted temperature field (in K) for the "TG03 - 3 bars" with a nozzle density of 16.6 sprays per meter and a curtain width of 0.24 m (irradiation from the right side)

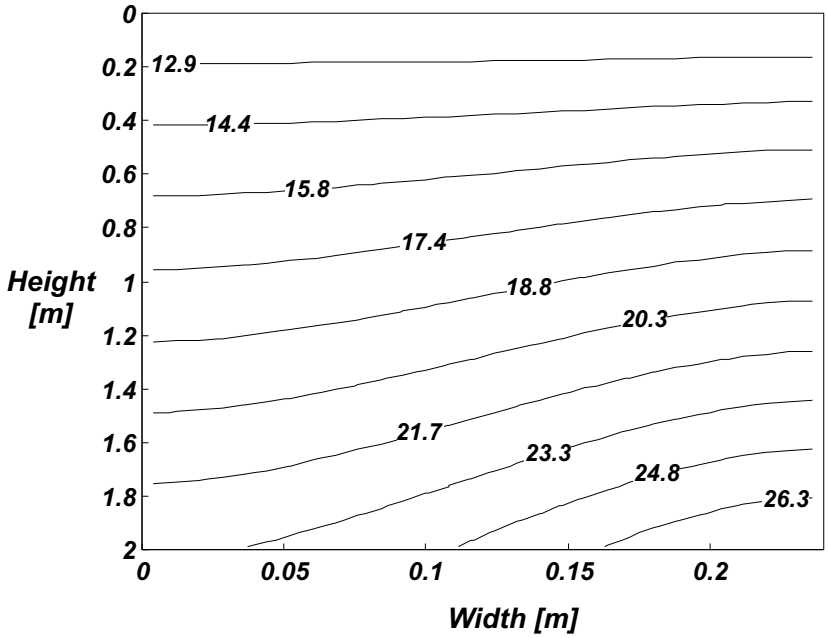

Figure 11: Predicted moisture field (in g of water / kg of air) for the "TG03 - 3 bars" with a nozzle density of 16.6 sprays per meter and a curtain width of 0.24 m (irradiation from the right side)

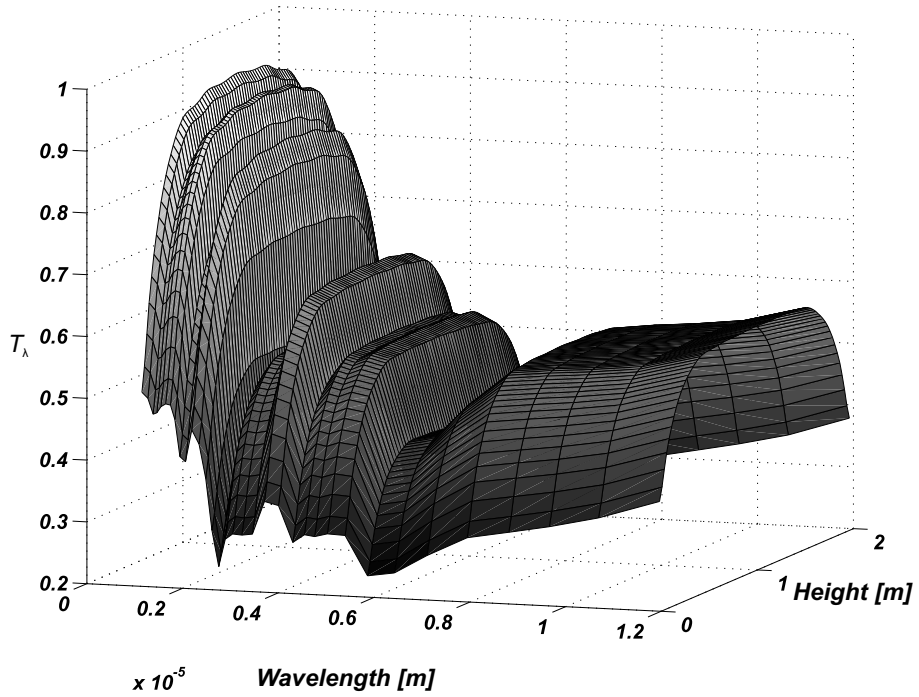

Figure 12: Spectral transmissivity in the plane opposite to the flame side ("TG03 - 3 bars" case with a nozzle density of 16.6 sprays per meter and a curtain width of 0.24 m)

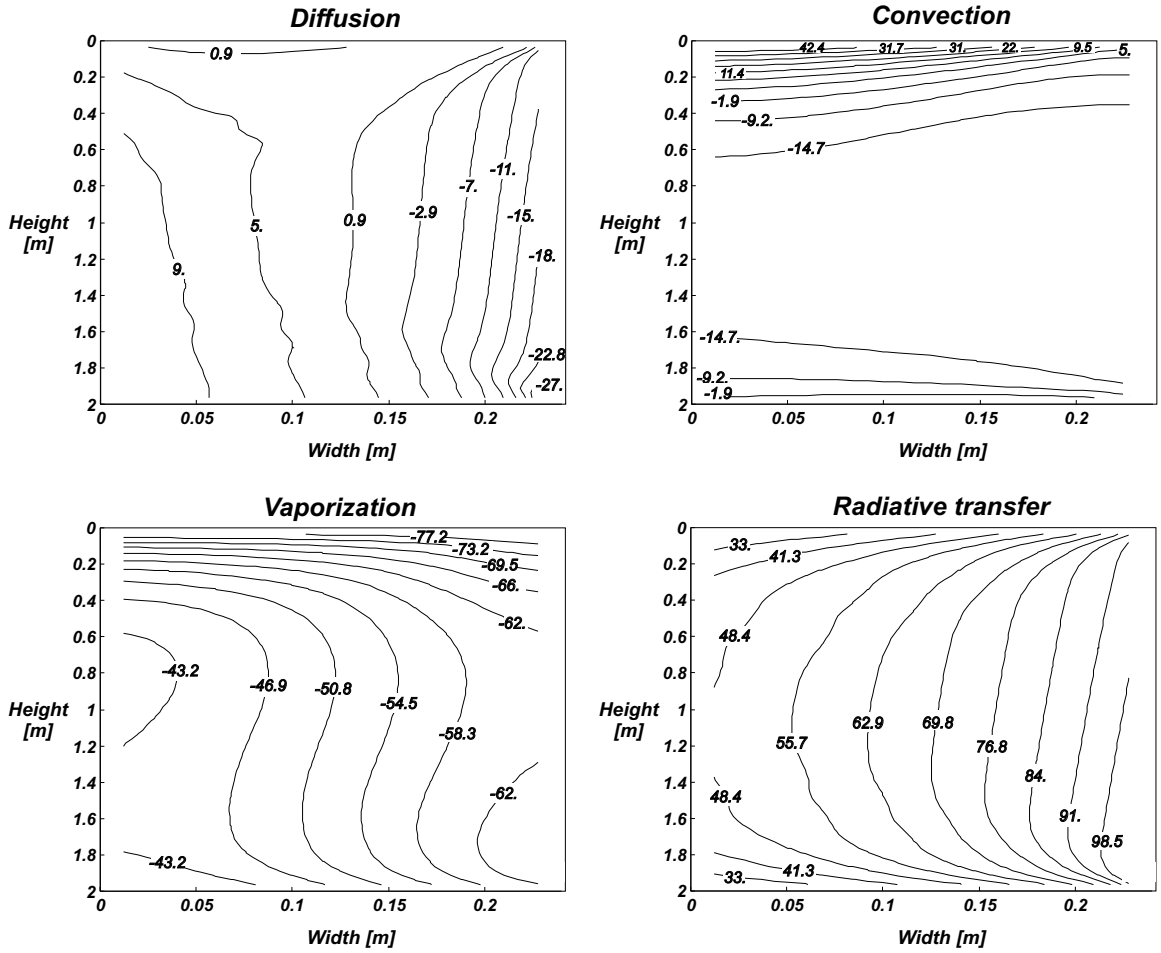

Figure 13: Contribution of the main transfer phenomena (in kW/m^3) for the "TG03 - 3 bars" case with a nozzle density of 16.6 sprays per meter and a curtain width of 0.24 m

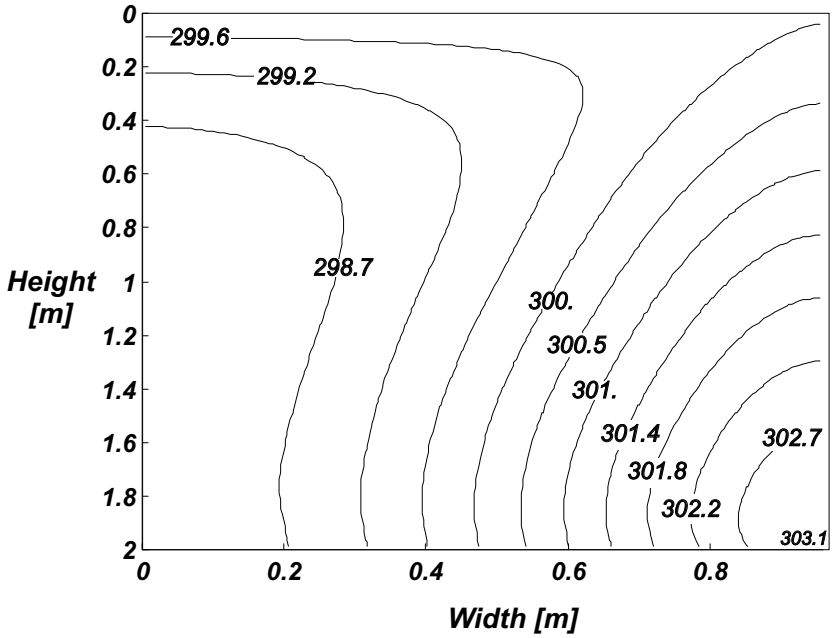

Figure 14: Predicted temperature field (in K) for the "TG03 - 3 bars" with a nozzle density of 4.2 sprays per meter and a curtain width of 0.96 m (irradiation from the right side)

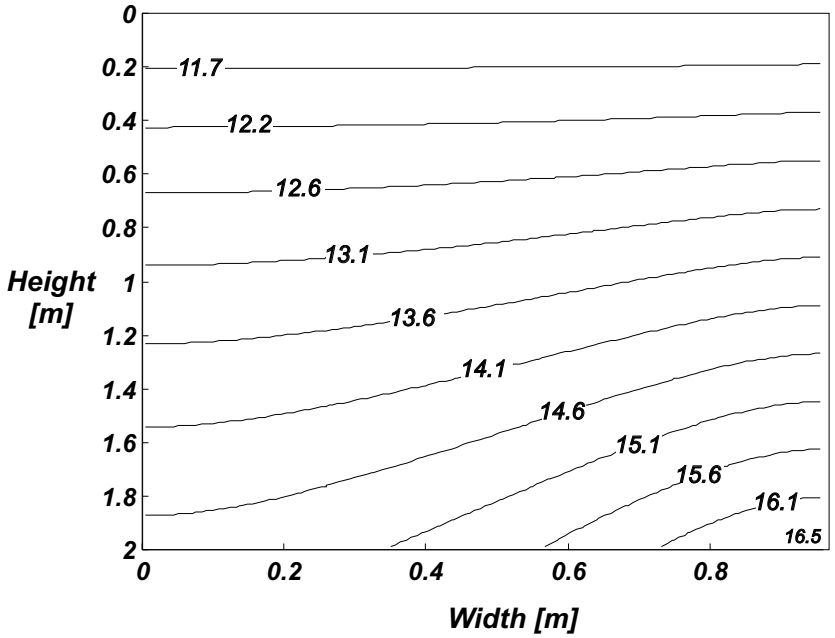

Figure 15: Predicted moisture field (in g of water / kg of air) for the "TG03 - 3 bars" with a nozzle density of 4.2 sprays per meter and a curtain width of 0.96 m (irradiation from the right side)

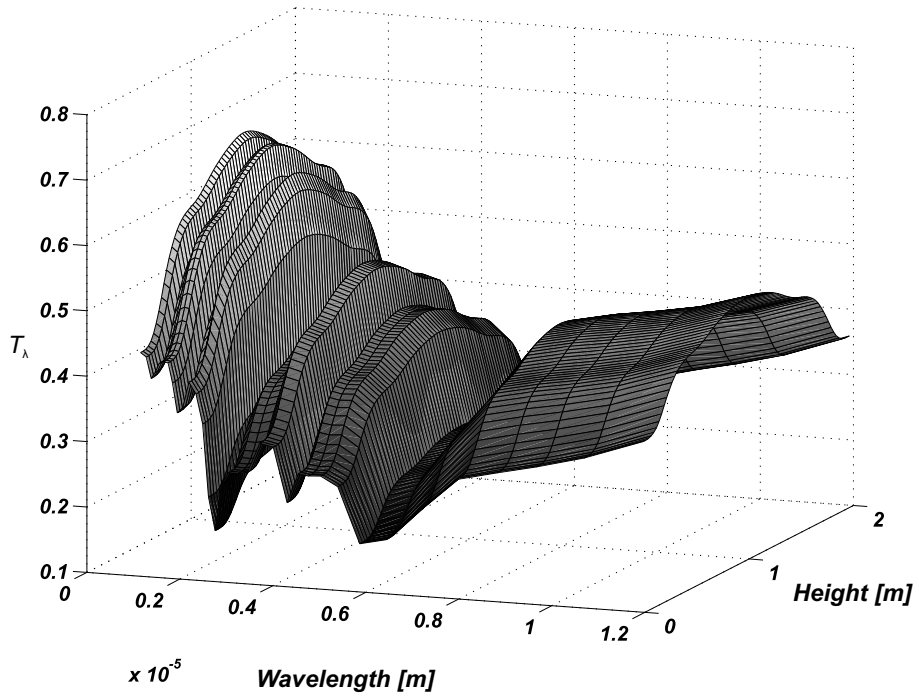

Figure 16: Spectral transmissivity in the plane opposite to the flame side ("TG03 - 3 bars" case with a nozzle density of 4.2 sprays per meter and a curtain width of 0.96 m)

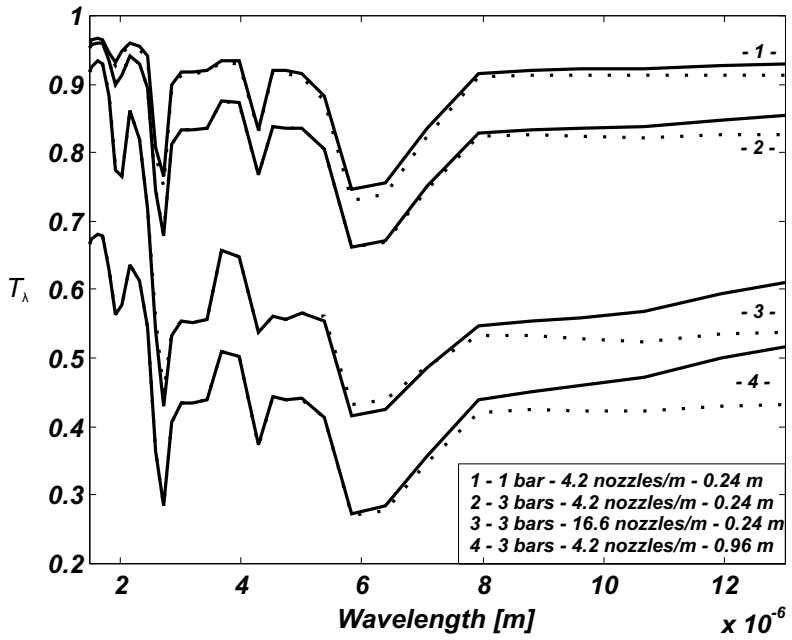

Figure 17: Spectral transmissivity as a function of wavelength at the mean vertical position $z = 1\ m$ for various spray configurations. Comparison with the prediction obtained with an uncoupled radiative transfer analysis (dotted lines)